

BitQ: Tailoring Block Floating Point Precision for Improved DNN Efficiency on Resource-Constrained Devices

Yongqi Xu¹, Yujian Lee², Gao Yi¹, Bosheng Liu¹, Yucong Chen³, Peng Liu¹, Jigang Wu¹, Xiaoming Chen⁴, Yinhe Han⁴

¹Computer Science and Technology, Guangdong University of Technology

²Faculty of Science and Technology, Beijing Normal University - Hong Kong Baptist University United International College

³School of Information Science and Engineering, Lanzhou University

⁴Institute of Computing Technology, Chinese Academy of Sciences

Abstract

Deep neural networks (DNNs) are powerful for cognitive tasks such as image classification, object detection, and scene segmentation. One drawback however is the significant high computational complexity and memory consumption, which makes them unfeasible to run real-time on embedded platforms because of the limited hardware resources. Block floating point (BFP) quantization is one of the representative compression approaches for reducing the memory and computational burden owing to their capability to effectively capture the broad data distribution of DNN models. Unfortunately, prior works on BFP-based quantization empirically choose the block size and the precision that preserve accuracy. In this paper, we develop a BFP-based bitwidth-aware analytical modeling framework (called “BitQ”) for the best BFP implementation of DNN inference on embedded platforms. We formulate and resolve an optimization problem to identify the optimal BFP block size and bitwidth distribution by the trade-off of both accuracy and performance loss. Experimental results show that compared with an equal bitwidth setting, the BFP DNNs with optimized bitwidth allocation provide efficient computation, preserving accuracy on famous benchmarks. The source code and data are available at <https://github.com/Cheliosoops/BitQ>.

Introduction

Recent advancements in deep neural networks (DNNs) have captured substantial interest from both academia and industry (Cheng et al. 2024; Liu et al. 2024b; Yuan et al. 2024b). The convergence of vast amounts of data and powerful computational prowess has fueled the rise of DNNs as a dominant force in modern computing (Hanna et al. 2024; Gao et al. 2023; Bassi et al. 2024). Nevertheless, one shortcoming of these DNNs pertains to the computational complexity and memory overhead. The expense associated with computation and memory access poses significant challenges when implementing state-of-the-art DNNs in practice on embedded platforms such as autonomous vehicles and mobile devices because of the limited hardware resources (Zheng, Zhang, and Jin 2023; Liu et al. 2024a; Clements and Lao 2024). To address such challenge, among the array of compression techniques aimed at enhancing model efficiency, block floating point (BFP) quantization (Drumond et al. 2018a; Kosson and Jaggi 2024; Akkad, Mansour, and Inaty 2023) emerges as a prominent strategy for reducing

both the memory footprint and computational burden. The BFP-based numerical representation has recently been established and deployed by the industry for the upcoming AI infrastructure (Yuan et al. 2024c).

BFP quantization provides a compromise between floating-point and fixed-point formats by grouping multiple floating point numbers into a block and replacing the data format with a shared exponent while retaining their respective mantissa (Darvish Rouhani et al. 2023; Song et al. 2023; Lo and Liu 2023). The advantages of BFP quantization are in twofold: it enables the streamlined storage of scale factors per block instead of for each data point individually, and simplifies multiplication by applying scaling factors in blocks rather than individually. BFP quantization combines the advantages of floating-point precision with fixed-point efficiency, providing an appealing solution for applications that prioritize memory efficiency, precision, dynamic range, and computational speed.

To increase the effective arithmetic density and memory bandwidth, researchers develop low bitwidth BFP quantization to reduce the precision of both weights and activations (Jung et al. 2022). Different from only focusing on the mantissa component, some works reduce the bitwidth of both the exponent and mantissa components of BFP data representation (Lian et al. 2019; Drumond et al. 2018a). For example, Drumond et al. (Drumond et al. 2018a) develop hybrid BFP data representation to maximize fixed-point arithmetic and minimize the mantissa width requirements while preserving convergence. Lian et al. (Lian et al. 2019) implement 8-bit BFP quantization with a 5-bit block exponent for DNN deployments, achieving less than 1% accuracy loss. Different from prior works that only focus on bitwidth quantization, Nascimento et al. (Nascimento et al. 2023) analyze the accuracy and efficiency impact of block size on BFP quantization. To fully utilize the bitwidth BFP quantization, DBPS (Lee et al. 2023) involves a dynamic block size and precision scaling to minimize energy consumption. FAST (Zhang et al. 2022) adaptively selects the optimal precision for weights and activations in the calculation.

Previous BFP quantization variants have varying degrees of optimization deployed to servers and edge devices. Nevertheless, previous researches on BFP-based quantization empirically rely on particular BFP representation and the block size, but such quantization settings are not necessarily

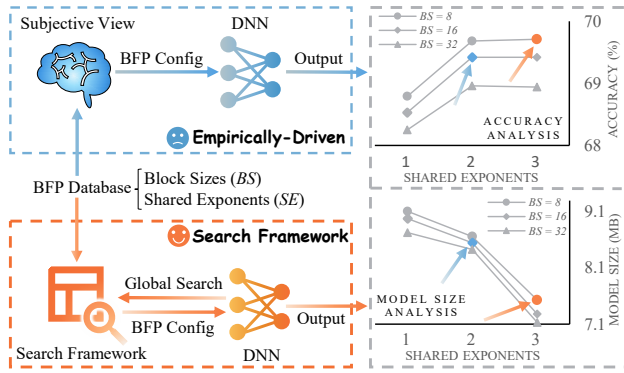


Figure 1: Comparison of BFP quantization configuration selection strategies: The figure illustrates the empirically-driven strategy in the upper section and the search framework strategy in the lower section, with line charts showcasing the performance gap on ResNet-18 (He et al. 2016) between the two selection methods.

the optimal solution in the quantization space, which offers limited opportunities for performance and efficiency gains. Specifically, Fig. 1 illustrates two selection strategies for BFP quantization parameters. Empirically-driven selection may result in suboptimal quantization outcomes, leading to inferior performance in terms of quantization loss and model size compared to search-based strategies. This is due to the large parameter search space in BFP quantization, where empirical configurations cannot robustly adapt to different DNNs. Therefore, searching for optimal BFP quantization parameters can effectively improve DNN efficiency.

To achieve high performance and energy efficiency, we provide a bitwidth-aware analytical searching framework (called “BitQ”) to fully exploit the BFP quantization for resource-constrained devices. While ensuring the quantitative loss is acceptable, we notice the data movement is a key bottleneck and dominates the energy consumption of DNN inference on resource-constrained devices (Ivanov et al. 2021; Chen et al. 2014; Gao et al. 2024). For example, the memory access occupies $> 90\%$ of the total energy for representative DNN deployments (Chen et al. 2014). Based on this observation, we formulate and resolve an optimization problem to identify the optimal BFP quantization configuration. Specifically, the model accuracy and the data movement volume can be utilized as the trade-off for the exploration of BFP quantization configurations. We develop a BFP-based modeling approach that can fully explore the data reuse of DNNs when evaluating the data movement volume. Experimental results based on image classification, object detection, and scene segmentation applications demonstrate that BitQ outperforms the state-of-the-art baselines.

The contributions of this work are summarized as follows.

- We propose a BFP-based bitwidth-aware analytical searching framework (named “BitQ”) tailored for optimizing DNN inference on embedded platforms by the trade-off between accuracy and data movement volume.
- We involve formulating and solving an optimization

problem to pinpoint the BFP block size and bitwidth distribution, carefully balancing accuracy with performance considerations by taking the block size into account, bitwidth configuration, and data reuse.

- Experimental results demonstrate that our optimized bitwidth allocation approach for BFP DNNs outperforms state-of-the-art baselines, delivering better computational efficiency and decreased memory access demands, preserving the accuracy.

Related Work

In embedded platforms, there are significant advantages in terms of decreased latency and enhanced energy efficiency through various forms of model compression. Pruning (Bai et al. 2023) and quantization (Kuzmin et al. 2024) are two widely employed techniques in practice. Pruning techniques primarily focus on the removal of individual parameters from DNNs. While pruning is theoretically interesting, it poses greater implementation challenges within the hardware configurations (Ma et al. 2020). On the other hand, quantization decreases the bitwidth for weights and network calculations, resulting in both predictable memories saving and the reduction of necessary computation.

The objective of DNN quantization is to quantize both weights and activations, enabling efficient calculation by leveraging limited hardware resources, which are faster and more memory-efficient compared with the standard FP32 format. There are two representative quantization formats: fixed-point and block floating point data representation (Yu et al. 2023; Akkad, Mansour, and Inaty 2023). Fixed-point numbers are treated as integers in hardware, facilitating simple and fast operations, but incorporating a scaling offset enabling limited fractional precision. Differently, BFP quantization involves grouping several values with a shared exponent while preserving individual mantissa. Based on the shared exponent, BFP quantization can overcome the limited numerical range encountered by fixed-point arithmetic. Among various bitwidths of BFP formats, both 16-bit and 8-bit quantization are widely deployed and utilized, owing to their efficiency in terms of memory storage, processing speed, and overall computational performance (Yuan et al. 2024a; Lian et al. 2019).

Recently, variant algorithms based on BFP quantization have effectively improved quantization performance. HBFP (Drumond et al. 2018b) is a hybrid approach combining BFP for dot products and floating point for other operations, offering high accuracy and superior hardware density. To provide adaptive BFP configurations for memory and calculation efficiency, DBPS (Lee et al. 2023) and FlexBlock (Noh et al. 2023) incorporate dynamic block sizes and scalable BFP quantization precision to reduce energy consumption. FAST (Zhang et al. 2022) dynamically chooses the optimal BFP precision for both activations and weights during calculation. Additionally, BSFP (Lo et al. 2023) achieves high computation efficiency by quantizing each weight vector as a superposition of multiple subword vectors with scaling factors in low-bit floating-point (LBFP), effectively fitting the weight vector distribution.

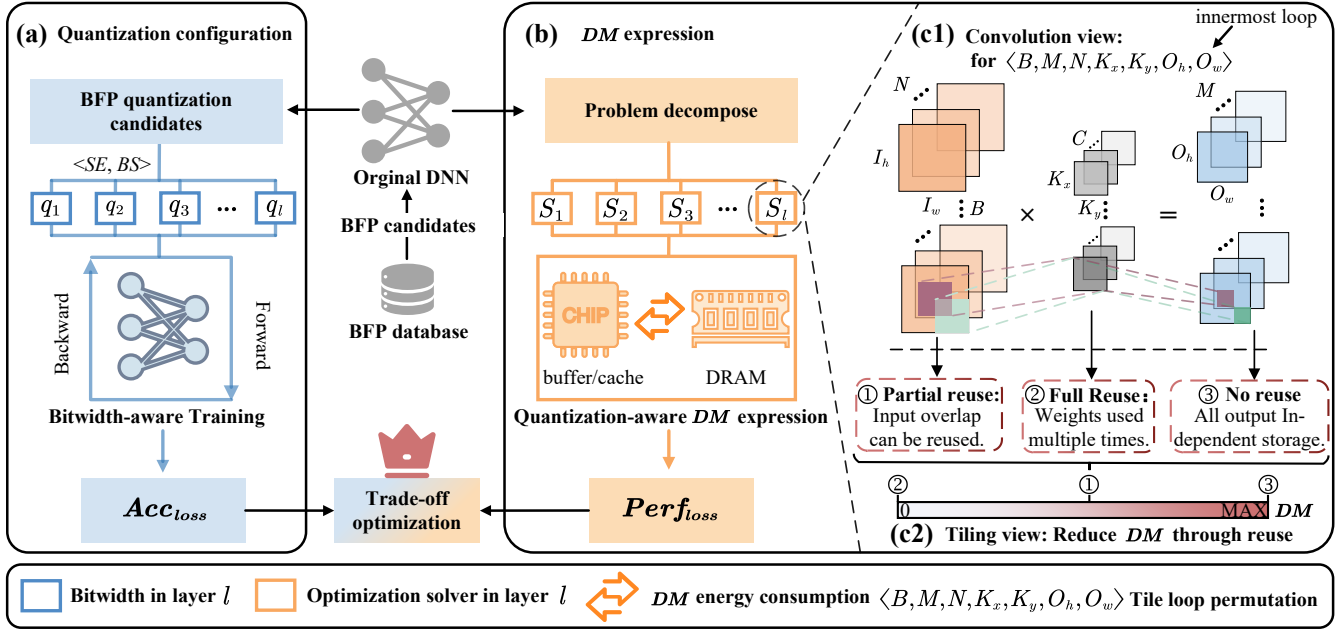


Figure 2: Workflow of the trade-off optimization of BitQ. (a) BFP quantization configuration. (b) Data movement (DM) expression. And (c) basis of convolution (c1) and data reuse in tiling (c2).

Methodology

This section outlines the BitQ workflow and its 3 key components: BFP quantization configuration, bitwidth-aware data movement expression, and trade-off optimization.

Workflow

Fig. 2 depicts the workflow of BitQ, which consists of three stages: BFP quantization configuration, bitwidth-aware data movement (DM) expression, and trade-off optimization. The BFP quantization configuration stage provides a set of DNN model accuracy loss after different BFP quantization configurations. The bitwidth-aware DM expression stage provides the data movement of convolutions. The trade-off optimization stage finds the best BFP quantization configuration based on the minimization of the objective function (\mathcal{O}), which is formulated as:

$$\min : \mathcal{O} = Acc_{loss}(SE, BS) + \alpha \cdot Perf_{loss}(SE, BS, \vec{I}, \vec{P}) \quad (1)$$

where Acc_{loss} denotes the accuracy loss at the BFP quantization configuration stage. $Perf_{loss}$ corresponds to the performance loss related to data movement in the DM expression stage. α serves as a balance factor for these losses. SE is the bitwidth of the shared exponent. BS reflects the block size of the shared exponent component. Input activations, output activations, and filter weights each have their designated SE and BS . \vec{I} signifies the tiling size. $\vec{P} = (\vec{p}_1, \dots, \vec{p}_l)$ denotes the loop permutations for tiling in the l -th convolution layer.

BFP Quantization Configuration

Fig. 2(a) depicts the BFP quantization configuration process, producing a range of accuracy candidates across different BFP quantization setups. The accuracy loss is generated by training. Each convolution layer within a DNN model is assigned a distinct bitwidth size that incorporates shared exponents and block sizes ($\langle SE, BS \rangle$) throughout the training process. Input activations, output activations, and filter weights are individually tailored with their specific $\langle SE, BS \rangle$ configurations.

Fig. 3 depicts the fundamental organization of BFP data representation. Fig. 3(a) illustrates the BFP data representation under 8-bit and 16-bit data widths, where each data block shares the same exponents. For example, in the 8-bit BFP data representation (with a block size of $BS = 2$, shared exponent of $SE = 3$, and mantissa $m = 4$), two data points share a common exponent. Fig. 3(b) illustrates the conversion process from original floating-point data to BFP representation, involving two key steps. Initially, it identifies the maximum exponent within a block size to serve as the shared exponent. Subsequently, it adjusts the mantissa through a shifting operation, refining the mantissa by subtracting individual mantissa values from the mantissa associated with the shared exponent.

Bitwidth-aware Data Movement Expression

Fig. 2(b) depicts the stage of bitwidth-aware data movement (DM) expression, aiming to compute data movement for specific BFP configurations. The objective is to boost inference efficiency by reducing energy consumption. Since data movement plays a vital role in energy usage, we employ DM as a measure to evaluate inference efficacy. In partic-

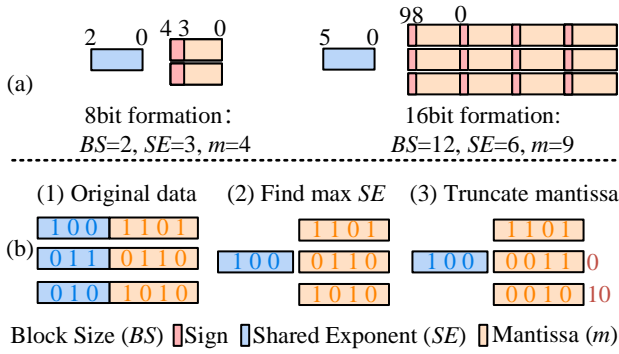


Figure 3: BFP data representation. (a) Illustration of 8-bit and 16-bit BFP data representation. (b) Process of generating BFP data from original data.

ular, we establish the connection between performance decline ($Perf_{loss}$ from Equation (1)) and DM , formulated as:

$$Perf_{loss} = \frac{DM_{sum}}{DM_{max}} \quad (2)$$

$$DM_{sum} = \sum_{1 \leq l \leq L} DM_l \quad (3)$$

where DM_{sum} identifies the total volume of data movement across all convolution layers, as outlined in Equation (3). DM_l denotes the data movement within the l -th convolution layer ($1 \leq l \leq L$), where L refers to the total number of convolution layers. DM_{max} corresponds the maximum value attained by DM_{sum} among various potential solutions encompassing different BFP quantization formats. The expression for the data movement in the l -th convolution layer (DM_l) is defined as,

$$DM_l = \sum DM_i \quad (4)$$

where DM_i identifies the data movement volume in the innermost loop of Fig. 2(c1), calculated as,

$$DM_i = \begin{cases} It_i \times DF_t(q_i, q_o, q_w), & \text{no reuse} \\ DF_t(q_i, q_o, q_w) + \\ (It_i - 1) \times DF_n(q_i, q_o, q_w), & \text{partial reuse} \\ 0, & \text{full reuse} \end{cases} \quad (5)$$

where DF_t is the data volumes of a single tile. DF_n signifies the effective volumes of new data exchanged between two consecutive tiles when data is partially reused. It_i denotes the iteration count within the innermost loop of a convolution. q_i , q_o , and q_w refer to the bitwidths of input activations, output activations, and filter weights. These can be computed as,

$$q_x = \begin{cases} (q_b - SE) + \frac{SE}{BS \cdot I_h \cdot I_w}, & x = i \\ (q_b - SE) + \frac{SE}{BS \cdot O_h \cdot O_w}, & x = o \\ (q_b - SE) + \frac{SE}{BS \cdot K_x \cdot K_y}, & x = w \end{cases} \quad (6)$$

where q_b denotes the overall bitwidth of data (e.g., 16-bit or 8-bit ($q_b = 16$ or $q_b = 8$)). q_x comprises a signed mantissa

and a shared exponent, where the mantissa can be derived from $q_b - SE$, and the shared exponent is determined by the block size BS .

For a convolution layer, we account for data reuse effects in data movement. Fig. 2(c2) illustrates three forms of data reuse, denoted as ①, ②, and ③. In the first scenario ①, there is no data reuse due to the lack of overlap in input activations when calculating adjacent output activations. Scenario ② showcases partial input activation reuse resulting from convolution with a specific stride size. Scenario ③ displays complete data reuse where the kernel size is smaller than the input feature maps, allowing full reutilization for output activations. Consequently, DM_i encompasses these three scenarios based on distinct data reuse patterns: no reuse during current computation, partial reuse due to convolution with a stride size, and complete data reuse eliminating the need for data movement.

Trade-off Optimization

The trade-off optimization involves two key steps: identifying the optimal data movement as well as considering data reuse and striving for the most favorable solution for the final outcomes.

Data Movement Optimization. Within a specific memory setting, configuration of the quantization, and tiling loop permutation for the l -th convolution layer ($\langle SE, BS, \vec{p}_l \rangle$), the optimization sub-problem aims to seek the best tiling size I_l . The minimum cost of DM_l can be articulated as,

$$\min : DM_l \quad \text{s.t.} \quad \sum DF_t(q_i, q_o, q_w) \leq MC \quad (7)$$

where MC denotes the memory capacity constraint on embedded platforms. The calculation of DM_l aligns with Equation (4). DF_t encompasses the data footprint volume of three tiles (e.g., tiles of input activations, output activations, and filter weights), computed based on Fig. 2(c2).

To minimize the total data movement cost, we optimize sub-problems within constraints. The optimization of each minimal single-level tiling problem, considering the constraint of MC , can be realized through nonlinear solvers (Wachter et al. 2006), which utilizes the feasible region to approximate the global optimum.

Optimal Solution Search. The trade-off optimization phase (the last stage of Fig. 2) focuses on seeking the best solution for the DNN inference while minimizing accuracy loss. The design space encompasses three parameter groups: BFP quantization strategies (SE, BS); loop permutations P ; and tiling sizes I .

To identify the optimal solution, we have formulated an objective function that guides exploration within the design space, to balance model accuracy loss with inference performance. The objective function, as outlined in Equation (1), facilitates the simultaneous minimization of accuracy and performance losses. Additionally, a trade-off factor (α) is employed to navigate the balance between model accuracy and inference efficiency.

Task	Model	Dataset
Image Classification	GoogLeNet (Szegedy et al. 2015)	ImageNet-1K (Deng et al. 2009)
	ResNet-18 (He et al. 2016)	
	ECA-MobileNetV2 (Wang et al. 2020)	
	ConvNeXt-L (Liu et al. 2022)	
Object Detection	YOLOv8 (Jocher et al. 2023)	COCO2017 (Lin et al. 2014)
	ONE-PEACE (Wang et al. 2023)	COCO2017 (Lin et al. 2014)
Instance Segmentation	YOLOv8 (Jocher et al. 2023)	COCO2017 (Lin et al. 2014)
	MaskDINO (Li et al. 2023)	ADE20K (Zhou et al. 2017)
Semantic Segmentation	MaskDINO (Li et al. 2023)	ADE20K (Zhou et al. 2017)
	ONE-PEACE (Wang et al. 2023)	ADE20K (Zhou et al. 2017)

Table 1: Characteristic of benchmarks and datasets.

Shared Exponents (SE)		Block Sizes (BS)
BitQ ₁₆	BitQ ₈	{1, 2, 4, 8, 16, 24, 32, 48}
{2, 3, 4, 5, 6, 7}	{2, 3, 4, 5, 6}	

Table 2: BFP quantization configuration candidates.

Evaluations

Experiment Setup

We conduct comprehensive experimental evaluations across diverse vision tasks, encompassing image classification on ImageNet-1K (Deng et al. 2009), object detection and instance segmentation on COCO2017 (Lin et al. 2014), and semantic segmentation on ADE20K (Zhou et al. 2017). Table 1 outlines the characteristics of the benchmarks and datasets.

Our approach includes two versions based on the size of q_b , namely BitQ₁₆ and BitQ₈ ($q_b = 16$ and $q_b = 8$, where q_b is the overall bitwidth of data), respectively. The balance factor α is set to be 0.2. The search process identifies the optimal configuration from Table 2 of BFP quantization candidates. We utilize a BFP quantizer for quantization-aware training, extending the training by 1,000 steps to compensate for the reduced data expression range due to quantization, following the recommended parameters.

We provide the original 32-bit floating-point data representation (labeled as "Original") for comparison. Additionally, we compare our approach against representative 16-bit BFP-based baselines, including DBPS (Lee et al. 2023) and Flexblock (Noh et al. 2023), as well as 8-bit BFP-based baselines, FAST (Zhang et al. 2022) and BSFP (Lo et al. 2023). The performance of the baselines comes from the results reported in the literature and our own reproductions.

The evaluation is conducted using a 2.90 GHz Intel i7-10700F CPU and an NVIDIA V100 graphics card. Models are quantified, trained, and validated on specific datasets over 10 rounds to derive the average performance metrics.

Accuracy Comparison

We conduct the accuracy evaluation involving representative four types of computer vision tasks. A geometric mean is supplied for accuracy evaluation within each task.

Table 3 lists the accuracy result. The proposed BitQ₁₆ and BitQ₈ show superior performance, winning all 14 and 12 out of 14 comparisons in the 16-bit and 8-bit bitwidth settings, respectively. Upon analyzing the baselines, we observe that DBPS (Lee et al. 2023) and FlexBlock (Noh et al. 2023) accelerate the training convergence by utilizing dynamic block



Figure 4: Visualization results of Original and BitQ₁₆₍₈₎ on downstream tasks.

sizes. However, since the final block sizes are empirically determined, the training convergence does not necessarily translate to optimal inference performance. FAST (Zhang et al. 2022) employs Stochastic Rounding to implement dynamic training for Transformers, which leads to improved accuracy in some Transformer-based models. The criterion-optimal quantization flow of BSFP (Lo et al. 2023) explores the quantization parameter space only partially, as the exhaustive search would be computationally prohibitive.

When compared with the Original baseline, BitQ₁₆ displays slight average accuracy decreases of 0.81%, 0.43%, 0.19%, and 0.58% across the same four benchmark groups. The slightly lower accuracy compared to the Original baseline is due to employing a smaller bitwidth for data representation. Compared with BitQ₈, BitQ₁₆ on average exhibits slightly better accuracy performance with increases of 0.55%, 0.49%, 0.33%, and 0.25% across the four groups of benchmarks, owing to its larger bitwidth for data representation. Despite reducing the bitwidth from 16-bit to 8-bit BFP data representation, the accuracy loss remains 0.55%, highlighting an efficient approach to reduce data movement.

Fig. 4 illustrates the visualization outcomes, contrasting BitQ₁₆₍₈₎ with the Original. We employ the images in the COCO2017 (Lin et al. 2014) for Object Detection and Instance Segmentation tasks and the image in the ADE20K (Zhou et al. 2017) dataset is utilized for Semantic Segmentation tasks. There is no significant difference by comparing the results produced by the original model and the original model applying the BitQ₁₆₍₈₎ quantization technique.

Energy Comparison

Fig. 5 shows the normalized energy consumption under four groups of benchmarks. The energy consumption is calculated based on the volume of data movement:

$$Energy = DM_S \times E_S + DM_D \times E_D \quad (8)$$

where DM_S and DM_D indicate the quantities of data movement in static random access memory (SRAM) and dynamic random access memory (DRAM), respectively. E_S and E_D

Task	Metric	Model	32-bit	16-bit			8-bit		
			Original	DBPS	FlexB	BitQ ₁₆	FAST	BSFP	BitQ ₈
Image Classification	Top-1 Acc.	GoogLeNet	67.79%	66.71%	66.58%	67.49%	66.31%	66.54%	66.58%
		ResNet-18	69.70%	68.42%	68.29%	69.83%	68.52%	69.67%	69.71%
		ECA-MobV2	72.56%	68.93%	70.25%	70.85%	70.15%	69.63%	69.85%
		ConvNeXt-L	85.82%	83.85%	83.87%	84.31%	83.82%	84.18%	84.26%
		Gmean_C	73.65%	71.67%	71.94%	72.84%	71.89%	72.20%	72.29%
Object Detection	Box AP	YOLOv8	37.30%	36.71%	36.28%	36.78%	36.36%	36.47%	36.50%
		ONE-PEACE	60.40%	59.47%	59.34%	60.14%	59.27%	59.23%	59.35%
		Gmean_O	47.46%	46.72%	46.40%	47.03%	46.42%	46.48%	46.54%
Instance Segmentation	Mask AP	YOLOv8	30.50%	30.03%	29.99%	30.19%	29.76%	29.88%	29.86%
		MaskDINO	46.30%	46.28%	46.30%	46.31%	45.72%	45.88%	45.99%
		Gmean_I	37.58%	37.28%	37.26%	37.39%	36.89%	37.03%	37.06%
Semantic Segmentation	mIoU	MaskDINO	48.73%	48.28%	48.13%	48.37%	48.26%	48.15%	48.34%
		ONE-PEACE	62.27%	61.27%	61.36%	61.42%	60.34%	60.37%	60.91%
		Gmean_S	55.09%	54.39%	54.34%	54.51%	53.96%	53.91%	54.26%

*ECA-MobV2 is denoted as ECA-MobileNetV2 (Wang et al. 2020), and FlexB as FlexBlock (Noh et al. 2023).

Table 3: Validation accuracy metrics. Gmean_C, Gmean_O, Gmean_I, and Gmean_S identify the geometric mean of different models in image classification, object detection, instance segmentation, and semantic segmentation tasks, respectively. The bold data indicate the best value under 16-bit and 8-bit bitwidth settings.

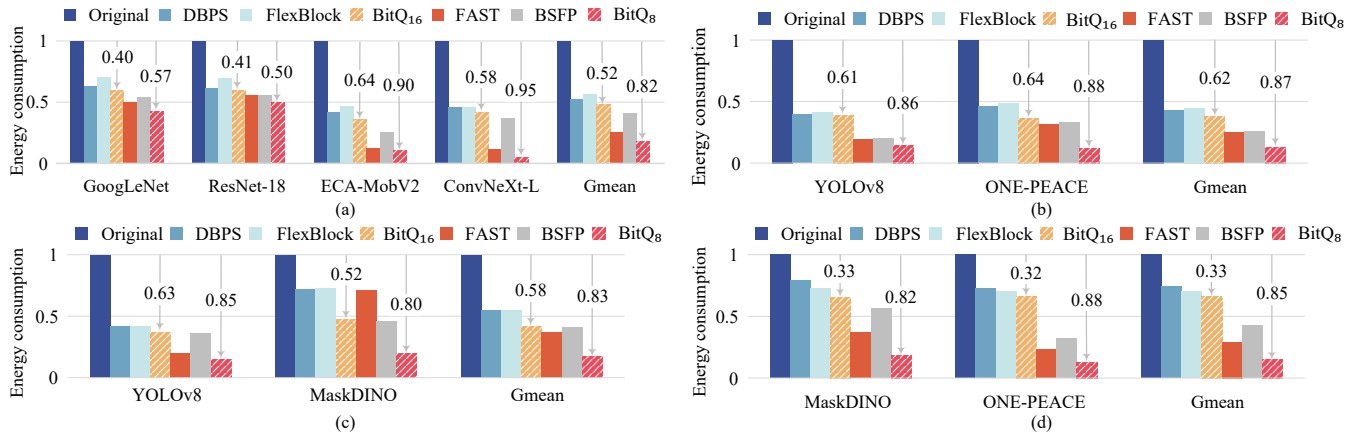


Figure 5: Normalized energy comparison under (a) image classification, (b) object detection, (c) instance segmentation, and (d) semantic segmentation. Less energy consumption is preferable. Gmean identifies the geometric mean across various models for corresponding visual tasks.

denote the energy consumption per unit of data movement in SRAM and DRAM, respectively. $E_S = 0.16$ pJ/bit and $E_D = 20$ pJ/bit (Horowitz 2014). To provide a visual comparison, all energy consumption values are normalized to the Original baseline, where the energy consumption is set to 1.

When compared to Original, BitQ₁₆ averages energy consumption of 0.52 \times , 0.62 \times , 0.58 \times , and 0.33 \times for the four benchmark groups. And BitQ₈ uses 0.82 \times , 0.87 \times , 0.83 \times , and 0.85 \times of the energy across the same four benchmark groups when compared with the Original baseline. The better energy saving of BitQ₁₆ and BitQ₈ compared to the baseline with the same bitwidth setting results from their effective quantization exploration for energy saving, as the shared exponent does not require reloading after its initial load-

ing, and the data for inference calculation is fully reused. Compared with BitQ₁₆, BitQ₈ on average consumes 0.30 \times , 0.25 \times , 0.25 \times , and 0.52 \times for the four groups of benchmarks. The reduced energy consumption comes from the reduction in data bitwidth from 16-bit to 8-bit data representation.

Sensitivity Analysis

Within the BitQ framework, a pivotal parameter is the loss balance factor α . Varied values of this parameter have the potential to impact inference performance and energy consumption diversely. Specifically, α plays a key role in the selection of BFP quantization parameters by striking a balance between accuracy and performance losses. We conduct the sensitivity analysis under different levels of α , by seven

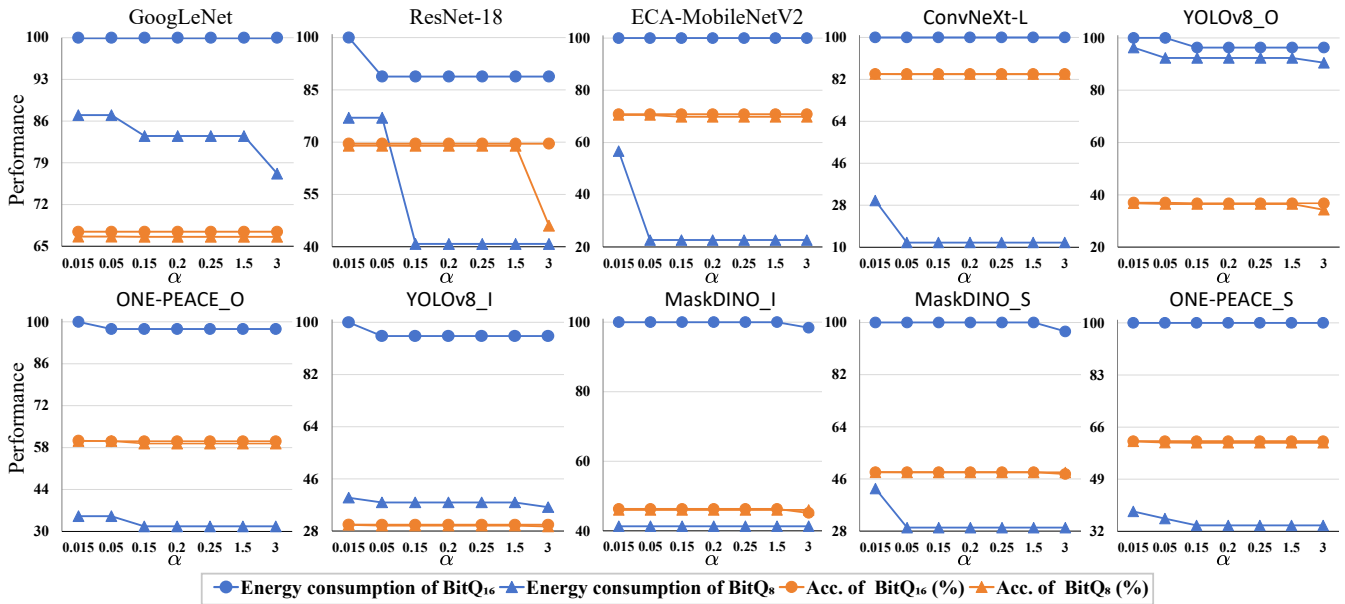


Figure 6: Accuracy and energy consumption sensitivity of $\text{BitQ}_{16(8)}$ with varying values of α . The suffixes $_{O}$, $_{I}$, and $_{S}$ indicate the model’s application scenarios in object detection, instance segmentation, and semantic segmentation, respectively. For a better display, we normalize the energy consumption values to a maximum of 100.

representative values ($\alpha \in \{0.015, 0.05, 0.15, 0.2, 0.25, 1.5, 3\}$, ranging from 0 to 3). We conduct the sensitivity analysis based on the same ten benchmarks (listed in Table 1) for both 16-bit and 8-bit BFP data representation.

Fig. 6 depicts the accuracy and energy consumption sensitivity of $\text{BitQ}_{16(8)}$ across different levels of α . Energy consumption is normalized with respect to $\alpha = 0.015$. To facilitate comparison, we scale the normalized energy consumption from 0 to 100, aligning both accuracy and normalized energy consumption on a common scale for clarity.

It can be observed from Fig. 6 that: 1) when α ranges from 0.05 to 3, BitQ achieves identical energy saving; 2) BitQ attains equivalent accuracy performance when α ranges from 0.015 to 3. The experimental results also reflect that BitQ with 8-bit data representation achieves equivalent accuracy and energy advantages within a narrower α range (0.15–1.5 for 8-bit data representation compared to 0.05–3 for 16-bit data representation). After thorough analysis, considering the impact of various DNNs and datasets, we choose α as 0.2 as a balanced approach.

In summary, BitQ stands out as a better choice owing to its adept balance between energy saving and accuracy for DNN inference on resource-constrained devices.

Ablation Study

To further validate the effectiveness of BitQ, we conduct ablation analysis. Since BitQ consists of three components, we perform ablations on each module individually. The specific results are shown in Table 4. In the w/o QAT method, we omit quantization-aware training, selecting quantization parameters solely based on DM size. This results in suboptimal accuracy but minimizes energy consumption. Con-

Method	16-bit		8-bit	
	Acc.	Eng.	Acc.	Eng.
BitQ	69.83%	0.143J	69.71%	0.119J
w/o QAT	66.82%	0.121J	31.74%	0.066J
w/o DM Expression	69.84%	0.197J	69.73%	0.142J
w/o Trade-off	69.43%	0.175J	68.84%	0.136J

*Eng. is denoted as energy consumption.

Table 4: Ablation results of BitQ on ResNet-18.

versely, in the w/o DM Expression method, we exclude data movement simulation during inference, leading to quantization parameters chosen solely for accuracy. While this method achieves optimal accuracy, it increases energy consumption. In the w/o Trade-off method, we independently consider accuracy loss and performance loss, using a Pareto optimal solution for parameter configuration. This method often fails to balance the two, resulting in suboptimal outcomes. Across all ablation settings, the BitQ algorithm consistently yields superior results.

Conclusion

We present a block floating point (BFP) based bitwidth-aware analytical modeling framework for optimizing DNN inference on resource-constrained devices. We establish and address an optimization challenge to determine the best BFP quantization configurations. Experimental results demonstrate that BitQ can achieve better energy saving, preserving accuracy loss on representative benchmarks.

References

- Akkad, G.; Mansour, A.; and Inaty, E. 2023. Embedded deep learning accelerators: A survey on recent advances. *IEEE Transactions on Artificial Intelligence*.
- Bai, S.; Chen, J.; Shen, X.; Qian, Y.; and Liu, Y. 2023. Unified Data-Free Compression: Pruning and Quantization without Fine-Tuning. In *Proceedings of the IEEE/CVF International Conference on Computer Vision*, 5876–5885.
- Bassi, P. R.; et al. 2024. Improving deep neural network generalization and robustness to background bias via layer-wise relevance propagation optimization. *Nature Communications*, 15(1): 291.
- Chen, T.; Du, Z.; Sun, N.; Wang, J.; Wu, C.; Chen, Y.; and Temam, O. 2014. Diannao: A small-footprint high-throughput accelerator for ubiquitous machine-learning. *ACM SIGARCH Computer Architecture News*, 42(1): 269–284.
- Cheng, L.; Gu, Y.; Liu, Q.; Yang, L.; Liu, C.; and Wang, Y. 2024. Advancements in Accelerating Deep Neural Network Inference on AIoT Devices: A Survey. *IEEE Transactions on Sustainable Computing*.
- Clements, J.; and Lao, Y. 2024. Resource Efficient Deep Learning Hardware Watermarks with Signature Alignment. In *Proceedings of the AAAI Conference on Artificial Intelligence*, volume 38, 11651–11659.
- Darvish Rouhani, B.; Zhao, R.; Elango, V.; Shafipour, R.; Hall, M.; Mesmakhosroshahi, M.; More, A.; Melnick, L.; Golub, M.; Varatkar, G.; et al. 2023. With shared microexponents, a little shifting goes a long way. In *Proceedings of the 50th Annual International Symposium on Computer Architecture*, 1–13.
- Deng, J.; Dong, W.; Socher, R.; Li, L.-J.; Li, K.; and Fei-Fei, L. 2009. ImageNet: A large-scale hierarchical image database. In *2009 IEEE Conference on Computer Vision and Pattern Recognition (CVPR)*, 248–255.
- Drumond, M.; Lin, T.; Jaggi, M.; and Falsafi, B. 2018a. Training dnns with hybrid block floating point. *Advances in Neural Information Processing Systems*, 31.
- Drumond, M.; LIN, T.; Jaggi, M.; and Falsafi, B. 2018b. Training DNNs with Hybrid Block Floating Point. In Bengio, S.; Wallach, H.; Larochelle, H.; Grauman, K.; Cesa-Bianchi, N.; and Garnett, R., eds., *Advances in Neural Information Processing Systems*, volume 31. Curran Associates, Inc.
- Gao, P.; Lee, Y.; Zhang, H.; Liu, X.; Hu, Y.; and Jing, G. 2024. Dynamic Identity-Guided Attention Network for Visible-Infrared Person Re-identification. *arXiv preprint arXiv:2405.12713*.
- Gao, W.; Sun, S.; Zheng, H.; Wu, Y.; Ye, H.; and Zhang, Y. 2023. OpenDMC: An open-source library and performance evaluation for deep-learning-based multi-frame compression. In *Proceedings of the 31st ACM International Conference on Multimedia*, 9685–9688.
- Hanna, M.; et al. 2024. How does GPT-2 compute greater-than?: Interpreting mathematical abilities in a pre-trained language model. *Advances in Neural Information Processing Systems*, 36.
- He, K.; Zhang, X.; Ren, S.; and Sun, J. 2016. Deep Residual Learning for Image Recognition. In *2016 IEEE Conference on Computer Vision and Pattern Recognition (CVPR)*, 770–778.
- Horowitz, M. 2014. 1.1 computing’s energy problem (and what we can do about it). In *2014 IEEE international solid-state circuits conference digest of technical papers (ISSCC)*, 10–14. IEEE.
- Ivanov, A.; Dryden, N.; Ben-Nun, T.; Li, S.; and Hoefler, T. 2021. Data movement is all you need: A case study on optimizing transformers. *Proceedings of Machine Learning and Systems*, 3: 711–732.
- Jocher; et al. 2023. Ultralytics YOLO.
- Jung, Y.; Kim, H.; Choi, Y.; and Kim, L.-S. 2022. Quantization-Error-Robust Deep Neural Network for Embedded Accelerators. *IEEE Transactions on Circuits and Systems II: Express Briefs*, 69(2): 609–613.
- Kosson, A.; and Jaggi, M. 2024. Multiplication-Free Transformer Training via Piecewise Affine Operations. *Advances in Neural Information Processing Systems*, 36.
- Kuzmin, A.; Nagel, M.; Van Baalen, M.; Behboodi, A.; and Blankevoort, T. 2024. Pruning vs Quantization: Which is Better? *Advances in Neural Information Processing Systems*, 36.
- Lee, S.; Choi, J.; Noh, S.; Koo, J.; and Kung, J. 2023. DBPS: Dynamic Block Size and Precision Scaling for Efficient DNN Training Supported by RISC-V ISA Extensions. In *2023 60th ACM/IEEE Design Automation Conference (DAC)*, 1–6. IEEE.
- Li, F.; Zhang, H.; Xu, H.; Liu, S.; Zhang, L.; Ni, L. M.; and Shum, H. 2023. Mask DINO: Towards A Unified Transformer-based Framework for Object Detection and Segmentation. In *2023 IEEE/CVF Conference on Computer Vision and Pattern Recognition (CVPR)*, 3041–3050.
- Lian, X.; Liu, Z.; Song, Z.; Dai, J.; Zhou, W.; and Ji, X. 2019. High-performance FPGA-based CNN accelerator with block-floating-point arithmetic. *IEEE Transactions on Very Large Scale Integration (VLSI) Systems*, 27(8): 1874–1885.
- Lin, T.-Y.; Maire, M.; Belongie, S.; Hays, J.; Perona, P.; Ramanan, D.; Dollár, P.; and Zitnick, C. L. 2014. Microsoft COCO: Common Objects in Context. In *Computer Vision – ECCV 2014*, 740–755. Cham: Springer International Publishing.
- Liu, R.; Wei, C.; Yang, Y.; Wang, W.; Yuan, B.; Yang, H.; and Liu, Y. 2024a. A Dynamic Execution Neural Network Processor for Fine-Grained Mixed-Precision Model Training Based on Online Quantization Sensitivity Analysis. *IEEE Journal of Solid-State Circuits*.
- Liu, Y.; Zhang, K.; Li, Y.; Yan, Z.; Gao, C.; Chen, R.; Yuan, Z.; Huang, Y.; Sun, H.; Gao, J.; et al. 2024b. Sora: A Review on Background, Technology, Limitations, and Opportunities of Large Vision Models.
- Liu, Z.; Mao, H.; Wu, C.; Feichtenhofer, C.; Darrell, T.; and Xie, S. 2022. A ConvNet for the 2020s. In *2022 IEEE/CVF Conference on Computer Vision and Pattern Recognition (CVPR)*, 11966–11976.

- Lo; et al. 2023. Block and subword-scaling floating-point (BSFP): An efficient non-uniform quantization for low precision inference. In *The Eleventh International Conference on Learning Representations*.
- Lo, Y.-C.; and Liu, R.-S. 2023. Bucket Getter: A Bucket-based Processing Engine for Low-bit Block Floating Point (BFP) DNNs. In *Proceedings of the 56th Annual IEEE/ACM International Symposium on Microarchitecture*, 1002–1015.
- Ma, X.; Guo, F.-M.; Niu, W.; Lin, X.; Tang, J.; Ma, K.; Ren, B.; and Wang, Y. 2020. Pconv: The missing but desirable sparsity in dnn weight pruning for real-time execution on mobile devices. In *Proceedings of the AAAI conference on artificial intelligence*, volume 34, 5117–5124.
- Nascimento, M. G. d.; Prisacariu, V. A.; Fawcett, R.; and Langhammer, M. 2023. HyperBlock Floating Point: Generalised Quantization Scheme for Gradient and Inference Computation. In *Proceedings of the IEEE/CVF Winter Conference on Applications of Computer Vision*, 6364–6373.
- Noh, S.-H.; Koo, J.; Lee, S.; Park, J.; and Kung, J. 2023. FlexBlock: A flexible DNN training accelerator with multi-mode block floating point support. *IEEE Transactions on Computers*.
- Song, L.; Chen, F.; Li, H.; and Chen, Y. 2023. ReFloat: Low-Cost Floating-Point Processing in ReRAM for Accelerating Iterative Linear Solvers. In *Proceedings of the International Conference for High Performance Computing, Networking, Storage and Analysis*, 1–15.
- Szegedy, C.; Liu, W.; Jia, Y.; Sermanet, P.; Reed, S.; Anguelov, D.; Erhan, D.; Vanhoucke, V.; and Rabinovich, A. 2015. Going deeper with convolutions. In *2015 IEEE Conference on Computer Vision and Pattern Recognition (CVPR)*, 1–9.
- Wachter, A.; et al. 2006. On the Implementation of an Interior-Point Filter Line-Search Algorithm for Large-Scale Nonlinear Programming. *Math. Program.*, 106(1): 25–57.
- Wang, P.; Wang, S.; Lin, J.; Bai, S.; Zhou, X.; Zhou, J.; Wang, X.; and Zhou, C. 2023. ONE-PEACE: Exploring One General Representation Model Toward Unlimited Modalities. *arXiv:2305.11172*.
- Wang, Q.; Wu, B.; Zhu, P.; Li, P.; Zuo, W.; and Hu, Q. 2020. ECA-Net: Efficient Channel Attention for Deep Convolutional Neural Networks. In *2020 IEEE/CVF Conference on Computer Vision and Pattern Recognition (CVPR)*, 11531–11539.
- Yu, C.; Chen, T.; Gan, Z.; and Fan, J. 2023. Boost vision transformer with gpu-friendly sparsity and quantization. In *Proceedings of the IEEE/CVF Conference on Computer Vision and Pattern Recognition*, 22658–22668.
- Yuan, S.; Chen, J.; Jiang, W.; Zhao, Z.; and Guo, S. 2024a. LHNetV2: A Balanced Low-Cost Hybrid Network for Single Image Dehazing. *IEEE Transactions on Multimedia*, 26: 8197–8209.
- Yuan, S.; Huang, J.; Shi, Y.; Xu, Y.; Zhu, R.; Lin, B.; Cheng, X.; Yuan, L.; and Luo, J. 2024b. MagicTime: Time-lapse Video Generation Models as Metamorphic Simulators. *arXiv:2404.05014*.
- Yuan, S.; Huang, J.; Xu, Y.; Liu, Y.; Zhang, S.; Shi, Y.; Zhu, R.; Cheng, X.; Luo, J.; and Yuan, L. 2024c. ChronoMagic-Bench: A Benchmark for Metamorphic Evaluation of Text-to-Time-lapse Video Generation. *arXiv preprint arXiv:2406.18522*.
- Zhang; et al. 2022. Fast: Dnn training under variable precision block floating point with stochastic rounding. In *2022 IEEE International Symposium on High-Performance Computer Architecture (HPCA)*, 846–860. IEEE.
- Zheng, B.; Zhang, H.; and Jin, L. 2023. Research on Multi-Person Pose Estimation Based on YOLO and Decoupled Multi-Level Feature Layers Fusion. In *Proceedings of the 5th ACM International Conference on Multimedia in Asia*, 1–7.
- Zhou, B.; Zhao, H.; Puig, X.; Fidler, S.; Barriuso, A.; and Torralba, A. 2017. Scene Parsing through ADE20K Dataset. In *2017 IEEE Conference on Computer Vision and Pattern Recognition (CVPR)*, 5122–5130.